USC–SIPI REPORT #239

Multiband Signal Reconstruction from Finite Samples

by

Xiang-Gen Xia, C.-C. Jay Kuo and Zhen Zhang

September 1993

Signal and Image Processing Institute
UNIVERSITY OF SOUTHERN CALIFORNIA
Department of Electrical Engineering-Systems
3740 McClintock Avenue, Room 404
Los Angeles, CA 90089-2564 U.S.A.

Multiband Signal Reconstruction from Finite Samples*

Xiang-Gen Xia† C.-C. Jay Kuo† Zhen Zhang‡

September 2, 1993

EDICS: SP 2.5.3

Abstract

The minimum mean-squared error (MMSE) estimator has been used to reconstruct a band-limited signal from its finite samples in a bounded interval and shown to have many nice properties. In this research, we consider a special class of band-limited 1-D and 2-D signals which have a multiband structure in the frequency domain, and propose a new reconstruction algorithm to exploit the multiband feature of the underlying signals. The concept of the critical value and region is introduced to measure the performance of a reconstruction algorithm. We show analytically that the new algorithm performs better than the MMSE estimator for band-limited/multiband signals in terms of the critical value and region measure. Finally, numerical examples of 1-D and 2-D signal reconstruction are given for performance comparison of various methods.

1 Introduction

Band-limited signal reconstruction from observed samples in a bounded interval is important in many signal and image processing and communication applications. It has been extensively studied by many researchers, say, [2]-[8], [10]-[15], [17]-[22], [25]-[29]. This problem can be generally stated as: given a band-limited signal $f(t)$ with bandwidth Ω, i.e. $\hat{f}(\omega) = 0$ for $|\omega| > \Omega$, we want to recover the singal $f(t)$ based on a limited number of samples $f(t_i)$, $i = 1, 2, \cdots, N$. The performance of existing reconstruction methods usually depends on the bandwidth Ω of $f(t)$. That is, algorithms perform poorlier when the bandwidth Ω becomes larger. However, it occurs in some applications that the spectrum of the signal $f(t)$ does not fill the whole bandwidth $[-\Omega, \Omega]$ but has a multiband structure in $[-\Omega, \Omega]$ as shown in Fig. 1. One such an example is signal transmission via frequency modulation with several carrier frequencies. Then, it is natural to seek an effective algorithm which reconstructs the signal by taking advantage of the multiband feature.

*This work was supported by the National Science Foundation Grant NCR-9205265, the National Science Foundation Young Investigator (NYI) Award ASC-9258396 and the Presidential Faculty Fellow (PFF) Award GER 93-50309.

†Signal and Image Processing Institute, Department of Electrical Engineering-Systems, University of Southern California, Los Angeles, CA 90089-2564. E-mail: xianggen@sipi.usc.edu and cckuo@sipi.usc.edu.

‡Communication Sciences Institute, Department of Electrical Engineering-Systems, University of Southern California, Los Angeles, CA 90089-2565. E-mail: zzhang@irving.usc.edu.

The multiband signal sampling problem has been recently addressed by Vaughan, Scott and White [24] and Beaty and Dodson [1]. An interesting result obtained is that it is possible to uniformly sample a multiband signal with a rate lower than the Nyquist rate based on the bandwidth Ω for its perfect reconstruction. The following reconstruction problem is studied in this research. Let $f(t)$ be a multiband signal with its Fourier spectrum as shown in Figure 1, where we assume that the bandwidth B_k and the center position C_k of each band indexed by $-m \leq k \leq m$ are known. Now, given a finite known samples $f(t_i)$, $t_i \in [-T, T]$ for certain $T > 0$, $i = 1, 2, \cdots, m$, we want to find an approximation $\tilde{f}(t)$ of $f(t)$ with $t \in [-\tau, \tau]$ where $\tau \geq T$.

In this work, we propose a new reconstruction algorithm for the above problem. To measure the performance of different methods, we introduce the concept of the critical region and the critical value. Roughly speaking, by the critical region, we mean the area that the reconstructed signal $\tilde{f}(t)$ provides a good approximation of the true signal $f(t)$. Then, we use the critical value to characterize the length or the area of the critical region for 1-D and 2-D signals, respectively. We obtain an explicit expression for the critical value of the new algorithm, and show that it is better than the one of the MMSE estimator where the multiband structure is not exploited. For modulated real signals, we can improve the reconstruction method furthermore so that its critical value is almost twice as large as the one applicable to general complex multiband signals with Fourier spectrum shown in Fig. 1. We also consider the extension of the new algorithm to 2-D multiband signals which has applications in image processing. Numerical examples in both 1-D and 2-D cases are given for performance comparison of various methods.

This paper is organized as follows. The MMSE estimator for band-limited signal signal reconstruction is briefly reviewed, and the concept of the critical value and region is introduced in Section 2. We study the 1-D and 2-D multiband signal reconstruction problems in Sections 3 and 4, respectively. We use some numerical examples to demonstrate the performance of the proposed algorithm in Section 5, and concluding remarks are given in Section 6.

2 Critical Regions and Values for Band-limited Signal Reconstruction

This section reviews some basic results of band-limited signal reconstruction [5], [12], [15], [25]. The main objective is to introduce the concept of critical region and its associated critical value for a given interpolant. We will examine both 1-D and 2-D cases.

Let $f(t)$ be an Ω band-limited (or simply ΩBLS) signal and $f(t_i)$, $i = 1, 2, \cdots, m$, be given

samples of $f(t)$. Then, the MMSE estimator for $f(t)$ is of the form (see Chen and Allebach [5]):

$$\Phi_m(t) = \sum_{k=1}^{m} a_k \frac{\sin \Omega(t - t_k)}{t - t_k}, \tag{2.1}$$

where coefficients $a_1, a_2, ..., a_m$ are determined by solving the linear system

$$\sum_{k=1}^{m} a_k \frac{\sin \Omega(t_n - t_k)}{t_n - t_k} = f(t_n), \quad n = 1, 2, ..., m. \tag{2.2}$$

It was proved in [5] that the MMSE estimator $\Phi_m(t)$ is identical to the minimum energy band-limited interpolant.

There are many ways to construct approximations of $f(t)$ from its samples $f(t_i)$ with $1 \leq i \leq m$. Let

$$\mathbf{N}_m f(t) = (f(t_1), f(t_2), ..., f(t_m)),$$

denote a mapping from the set B_Ω of all Ω band-limited signals to the m-D complex Euclidean space $\mathbf{C}^m$. Then, an *interpolant* $\Psi_m(t)$ is a function-valued mapping defined on the space of $\mathbf{N}_m f$ with $f \in B_\Omega$. Micchelli and Rivlin [15] proved that

$$\sup_{t\in[-\tau,\tau]} \sup_{f\in B_{\Omega,E}} |f(t) - \Phi_m(t)| \leq \sup_{t\in[-\tau,\tau]} \sup_{f\in B_{\Omega,E}} |f(t) - \Psi_m(t)|, \tag{2.3}$$

where $B_{\Omega,E}$ denotes the set of all Ω band-limited signals with energy less than or equal to 1, $\Phi_m(t)$ is the MMSE estimator in (2.1) and τ is an positive number such that $|t_i| \leq \tau$ for $i = 1, 2, \cdots, m$. The MMSE estimator is sometimes called the pointwise minimum-error estimator in the worst case due to the property (2.3).

Furthermore, we have the following error estimate for the MMSE estimator $\Phi_m(t)$ (see (13) in Kowalski [12])

$$|f(t) - \Phi_m(t)| < O\sqrt{E(f)} \frac{\Omega^{1/2}}{m(m\kappa)^m} \quad \forall t \in [-\tau, \tau], \tag{2.4}$$

where $O = e^{-1/12}(2\pi)^{1/2}$, $\kappa = \frac{1}{2e\tau\Omega}$ and $E(f)$ is the energy of f. Thus, given the number m of samples and the bandwidth Ω of $f(t)$, we can determine the condition on τ so that the error bound is small in the interval $[-\tau, \tau]$. It is clear from (2.4) that we need

$$m\kappa > 1, \quad \text{or} \quad \tau < \frac{m}{2e\Omega},$$

and a larger $m\kappa$ (or a smaller τ) implies a smaller error bound. The ratio

$$\Gamma_{\Phi_m} \triangleq \frac{m}{2e\Omega} \tag{2.5}$$

is called the *critical value* for the interpolant $\Phi_m(t)$ and the interval $[-\Gamma_{\Phi_m}, \Gamma_{\Phi_m}]$ is called the *critical region*. We conclude that the $\Phi_m(t)$ is a good approximation of $f(t)$ if $|t|$ belongs to the

critical region as shown in Fig. 2 (a). Different interpolants may have different critical regions, and we can use the critical value as one performance measure. In this paper, when we say that an interpolant $\Psi_1(t)$ is better than another one $\Psi_2(t)$, it is meant that

$$\Gamma_{\Psi_1} \geq \Gamma_{\Psi_2}.$$

That is, $\Phi_1(t)$ can approximate $f(t)$ better in a larger interval.

The MMSE estimator can also be extended to the 2-D case (see Chen and Allebach [5] for more details). Let $f(s,t)$ be (Ω_1, Ω_2) band-limited, that is, $\hat{f}(\omega_1, \omega_2) = 0$ when $|\omega_1| > \Omega_1$ or $|\omega_2| > \Omega_2$ so that

$$\begin{aligned} \hat{f}(\omega_1, \omega_2) &= \int_{-\infty}^{\infty}\int_{-\infty}^{\infty} f(s,t)e^{-j(s\omega_1+t\omega_2)}dsdt \\ &= \int_{-\Omega_2}^{\Omega_2}\int_{-\Omega_1}^{\Omega_1} f(s,t)e^{-j(s\omega_1+t\omega_2)}dsdt. \end{aligned}$$

Let $f(s_{i_1}, t_{i_2})$, $i_1 = 1, 2, \cdots, m_1$, $i_2 = 1, 2, \cdots, m_2$, be given samples of $f(s,t)$. Then, the MMSE estimator of $f(s,t)$ from these samples is

$$\Phi_{m_1 m_2}(s,t) = \sum_{i_1=1}^{m_1}\sum_{i_2=1}^{m_2} a_{i_1 i_2} \frac{\sin \Omega_1(s - s_{i_1})}{s - s_{i_1}} \frac{\sin \Omega_2(t - t_{i_2})}{t - t_{i_2}}, \tag{2.6}$$

where coefficients $a_{i_1 i_2}$ satisfy

$$\sum_{i_1=1}^{m_1}\sum_{i_2=1}^{m_2} a_{i_1 i_2} \frac{\sin \Omega_1(s_{n_1} - s_{i_1})}{s_{n_1} - s_{i_1}} \frac{\sin \Omega_2(t_{n_2} - t_{i_2})}{t_{n_2} - t_{i_2}} = f(s_{n_1}, t_{n_2}), \tag{2.7}$$

for $n_1 = 1, 2, \cdots, m_1$ and $n_2 = 1, 2, \cdots, m_2$. For the error estimation, Xia et al. [25] extended the error bound (2.4) and obtained the following results.

Proposition 1 *Let $f(s,t)$ be (Ω_1, Ω_2) band-limited. If $f(s,t) \in L^1(\mathbf{R}^2)$, that is,*

$$\int_{\mathbf{R}^2} |f(s,t)|dsdt < \infty,$$

then,

$$|f(s,t) - \Phi_{m_1 m_2}(s,t)| < O_1 \left(\frac{1}{m_1(m_1\kappa_1)^{m_1}} + \frac{1}{m_2(m_2\kappa_2)^{m_2}} \right), \ \forall |s| \leq \tau_1, \ |t| \leq \tau_2, \tag{2.8}$$

where

$$O_1 = \frac{8\sqrt{2}}{\pi^3} e^{\pi - \frac{1}{6}} \Omega_1 \Omega_2 \int_{\mathbf{R}^2} |f(s,t)|dsdt, \quad \textit{and} \quad \kappa_l = \frac{1}{2e\tau_l\Omega_l}, \ l = 1, 2.$$

and $|s_{i_1}| \leq \tau_1$ and $|t_{i_2}| \leq \tau_2$ for all possible i_1 and i_2 with arbitrarily given values of τ_1 and τ_2.

Proposition 2 *Let $f(s,t)$ be (Ω_1,Ω_2) band-limited. If its Fourier spectrum $\hat{f}(\omega_1,\omega_2)$ is second-order differentiable, then*

$$|f(s,t)-\Phi_{m_1m_2}(s,t)|<O_2\left(\frac{1}{m_1(m_1\kappa_1)^{m_1}}+\frac{1}{m_2(m_2\kappa_2)^{m_2}}\right),\ \forall\,|s|\le\tau_1,\ |t|\le\tau_2, \tag{2.9}$$

where

$$O_2=\frac{2\sqrt{2}}{\pi}e^{-\frac{1}{12}}\Omega_1\Omega_2\sum_{n_1,n_2}|b_{n_1n_2}|<\infty,\quad \textit{and}\quad \kappa_l=\frac{1}{2e\tau_l\Omega_l},\ l=1,2. \tag{2.10}$$

and $|s_{i_1}|\le\tau_1$ and $|t_{i_2}|\le\tau_2$ for all possible i_1 and i_2 with arbitrarily given values of τ_1 and τ_2. The values $b_{n_1n_2}$ in (2.9) are Fourier coefficients of $\hat{f}(\omega_1,\omega_2)$ in $[-\Omega_1,\Omega_1]\times[-\Omega_2,\Omega_2]$.

Although the constants O_1 and O_2 are different in error bounds (2.8) and (2.9), they have the same main term. Similar to the 1-D case, we can also determine the critical region for the interpolant $\Phi_{m_1m_2}$. To have $m_l\kappa_l>1$, $l=1,2$, we require

$$\tau_l<\frac{m_l}{2e\Omega_l}=\Gamma_{\Phi_{m_l}},\quad l=1,2,$$

which is the critical region of $\Phi_{m_1m_2}$. We plot the critical region in Fig. 2(b) as a square enclosed by the solid line, in which $\Phi_{m_1m_2}(s,t)$ provides a good approximation for $f(s,t)$. Furthermore, we choose

$$\Gamma_{\Phi_{m_1m_2}}\triangleq\frac{m_1m_2}{4e^2\Omega_1\Omega_2}=\Gamma_{\Phi_{m_1}}\Gamma_{\Phi_{m_2}} \tag{2.11}$$

to be the critical value corresponding to the area of a quarter of the critical region (i.e. the dark region in Fig. 2(b)). Thus, we can also measure the performance of an 2-D interpolant with its critical value.

3 1-D Multiband Signal Reconstruction

3.1 General Multiband Signals

We consider the reconstruction of a 1-D multiband signal $f(t)$ with its Fourier spectrum shown in Figure 1, where $B_k>0$ and C_k with $|k|\le K$, are known a priori and $C_k-C_{k-1}\ge B_k+B_{k-1}$. The $f(t)$ can be represented as

$$f(t)=\sum_{k=-K}^{K}f_k(t)e^{-jtC_k}, \tag{3.1}$$

where $f_k(t)$ is B_k band-limited. Since the bandwidth Ω of $f(t)$ is often much larger than each B_k of $f_k(t)$, the critical value of the MMSE estimator for $f(t)$ is much smaller than that for $f_k(t)$. This observation motivates us to use the MMSE estimator of $f_k(t)$ with $|k|\le K$ for the reconstruction of $f(t)$.

Let $S \triangleq \{t_1, t_2, \cdots, t_m\} \subset [-T, T]$ for certain $T > 0$ be the set of selected sampling points, and $S_k \triangleq \{t_{k1}, t_{k2}, \cdots, t_{km_k}\} \subset [-T, T]$ be the set of arbitrarily fixed m_k distinct points, where m_k satisfies

$$\sum_{k=-K}^{K} m_k = m.$$

Then, a new reconstruction interpolant can be obtained via

$$\Psi_m(t) = \sum_{k=-K}^{K} \sum_{i=1}^{m_k} a_{ki} \frac{\sin B_k(t - t_{ki})}{t - t_{ki}} e^{-jtC_k}, \tag{3.2}$$

where coefficients a_{ki} satisfy the following system

$$\sum_{k=-K}^{K} \sum_{i=1}^{m_k} a_{ki} \frac{\sin B_k(t_n - t_{ki})}{t_n - t_{ki}} e^{-jt_nC_k} = f(t_n), \quad n = 1, 2, \cdots, m. \tag{3.3}$$

Note that the points t_{ki} in S_k are arbitrarily chosen in $[-T, T]$ and may not be related to the sampling points in S.

It is clear from (2.5) that, to keep the critical value constant, the larger the bandwidth B_k of the kth signal $f_k(t)$ the more points m_k we need in S_k so that

$$\sum_{i=1}^{m_k} a_{ki} \frac{\sin B_k(t - t_{ki})}{t - t_{ki}}$$

approximates $f_k(t)$ well. Thus, we impose the size m_k of set S_k by the constraint

$$\frac{m_k}{B_k} = r, \quad k = -K, -K+1, \cdots, K, \tag{3.4}$$

where r is a positive constant. With (3.4) we have

$$r = \frac{\sum_{k=-K}^{K} m_k = m}{\sum_{k=-K}^{K} B_k} = \frac{m}{\sum_{k=-K}^{K} B_k}. \tag{3.5}$$

The following theorem gives an error bound for the reconstruction interpolant $\Psi_m(t)$ given by (3.2).

Theorem 1 *Let $f(t)$ be a multiband signal with parameters as stated before. If the coefficient matrix for unknowns a_{ki} in (3.3) is of full rank, then*

$$|f(t) - \Psi_m(t)| < Or \sum_{k=-K}^{K} \left(\frac{2e\tau}{r}\right)^{m_k}, \quad \text{for } t \in [-\tau, \tau], \tag{3.6}$$

where $\tau \geq T$, r is defined in (3.5) and O is a positive constant.

The proof of Theorem 1 is given in Appendix. The coefficient matrix in (3.3) often has a full rank. If not, one can adjust the points in S_k to make it a full rank matrix.

Based on the error bound (3.6), the critical value Γ_{Ψ_m} for the interpolant $\Psi_m(t)$ can be defined as

$$\Gamma_{\Psi_m} = \frac{r}{2e} = \frac{m}{2e\sum_{k=-K}^{K} B_k} = \frac{\Omega}{\sum_{k=-K}^{K} B_k}\Gamma_{\Phi_m}. \tag{3.7}$$

We see that the critical value Γ_{Ψ_m} is reciprocally related to the total size of occupied bands, i.e. $2\sum_{k=-K}^{K} B_k$. Furthermore, since $\sum_{k=-K}^{K} B_k \leq \Omega$, we have

$$\Gamma_{\Psi_m} \geq \Gamma_{\Phi_m}. \tag{3.8}$$

This means that the length of the critical interval of the interpolant Ψ_m given by (3.2) for an Ω band-limited signal with a multiband structure is always greater than or equal to that of its MMSE estimator Φ_m without exploiting the multiband feature. In addition, when the multiband signal $f(t)$ does not fully occupy the band $[-\Omega, \Omega]$, the critical value Γ_{Ψ_m} of our proposed method is strictly greater than the critical value Γ_{Φ_m} of the MMSE estimator. We call

$$\gamma_1 \triangleq \frac{\Omega}{\sum_{k=-K}^{K} B_k},$$

the *gain factor*. When the band $[-\Omega, \Omega]$ is fully occupied, the gain factor is 1 (no gain).

When all B_k are equal, the error bound in (3.6) can be simplified.

Corollary 1 *Let $f(t)$ be a multiband signal with parameters as before and $B_k = B$ for all k. If the coefficient matrix for unknowns a_{ki} in (3.3) is of full rank, then*

$$|f(t) - \Psi_m(t)| < O(2K+1)r\left(\frac{2e\tau}{r}\right)^{m/(2K+1)}, \quad \text{for } t \in [-\tau, \tau], \tag{3.9}$$

where

$$r = \frac{m}{(2K+1)B}.$$

3.2 Real Multiband Signals

As a special case of multiband signals $f(t)$ in (3.1), we assume all $f_k(t)$ and $f(t)$ to be real in this subsection. The signal $f(t)$ can be represented as

$$f(t) = \sum_{k=0}^{K} f_k(t)\cos(C_k t), \tag{3.10}$$

where $f_k(t)$ is real B_k band-limited for $k = 0, 1, 2, \cdots, K$. A typical Fourier spectrum for this class of signals is shown in Fig. 3, where $B_{-k} = B_k$.

For $f(t)$ given by (3.10), we can use another interpolant instead of the one in (3.2)-(3.3), i.e.

$$\tilde{\Psi}_m(t) = \sum_{k=0}^{K}\sum_{i=1}^{m_k} a_{ki}\frac{\sin B_k(t - t_{ki})}{t - t_{ki}}\cos(C_k t),$$

where t_{ki} with $i = 1, 2, \cdots, m_k$ are arbitrarily fixed distinct points in $[-T, T]$ for each k, $\sum_{k=0}^{K} m_k = m$ and a_{ki} are obtained via solving the system

$$\sum_{k=0}^{K} \sum_{i=1}^{m_k} a_{ki} \frac{\sin B_k(t_n - t_{ki})}{t_n - t_{ki}} \cos(C_k t_n) = f(t_n),\ n = 1, 2, \cdots, m.$$

We can derive an error bound for $\tilde{\Psi}_m(t)$ similar to that given in Theorem 1 as

$$|f(t) - \tilde{\Psi}_m(t)| < O\tilde{r} \sum_{k=0}^{K} \left(\frac{2e\tau}{\tilde{r}}\right)^{m_k}, \quad t \in [-\tau, \tau],$$

where O is as before and

$$\tilde{r} = \frac{m}{\sum_{k=0}^{K} B_k}.$$

In particular, if $B_k = B$ for $k = 0, 1, 2, \cdots, K$, we have a result similar to Corollary 1, that is,

$$|f(t) - \tilde{\Psi}_m(t)| < O\tilde{r} \left(\frac{2e\tau}{\tilde{r}}\right)^{m/(K+1)}, \quad t \in [-\tau, \tau].$$

The critical value for this case is

$$\Gamma_{\tilde{\Psi}_m} = \frac{m}{2e \sum_{k=0}^{K} B_k} = \frac{\sum_{k=-K}^{K} B_k}{\sum_{k=0}^{K} B_k} \Gamma_{\Psi_m} = \left(1 + \frac{\sum_{k=1}^{K} B_k}{\sum_{k=0}^{K} B_k}\right) \Gamma_{\Psi_m}. \tag{3.11}$$

Combining (3.8) and (3.11), we obtain

$$\Gamma_{\tilde{\Psi}_m} > \Gamma_{\Psi_m} \geq \Gamma_{\Phi_m} \quad \text{for} \quad K > 0.$$

Besides, it is straightforward to derive that

$$\Gamma_{\tilde{\Psi}_m} = \gamma_2 \Gamma_{\Phi_m},$$

where

$$\gamma_2 \triangleq \frac{\Omega}{\sum_{k=0}^{K} B_k}$$

is the gain factor of $\tilde{\Psi}_m$ with the MMSE estimate Φ_m as the reference. It is interesting to point out that γ_2 is always greater than 1 if $K > 0$. When the bandwidth B_0 of the base band is small with

$$\frac{\sum_{k=1}^{K} B_k}{\sum_{k=0}^{K} B_k} \approx 1,$$

we can simplify (3.11) to be

$$\Gamma_{\tilde{\Psi}_m} \approx 2\Gamma_{\Psi_m} \geq 2\Gamma_{\Phi_m},$$

so that the gain factor $\gamma_2 \approx 2$. This implies that the interpolant $\tilde{\Psi}_m$ for modulated real signals performs almost twice as well as the MMSE estimator Γ_{Φ_m}. This point will be demonstrated in numerical examples in Section 5.

4 2-D Multiband Signal Reconstruction

4.1 General Multiband Signals

Now, let us consider 2-D multiband signals $f(s,t)$ with $2K+1$ nonoverlaping multibands bounded by $[-\Omega_1,\Omega_1]\times[-\Omega_2,\Omega_2]$ as shown in Fig. 4, where each band with index $-K\le k\le K$ has the center frequencies C_{1k} and C_{2k} and bandwidths B_{1k} and B_{2k} along the frequency axes ω_1 and ω_1, respectively. We assume that these multiband parameters are known a priori. It is clear that

$$\sum_{k=-K}^{K} B_{1k}B_{2k}\le \Omega_1\Omega_2. \tag{4.1}$$

The 2-D multiband signal $f(s,t)$ can be represented by

$$f(s,t)=\sum_{k=-K}^{K} f_k(s,t)e^{-j(sC_{1k}+tC_{2k})}, \tag{4.2}$$

where $f_k(s,t)$ is (B_{1k},B_{2k}) band-limited while $f(s,t)$ is (Ω_1,Ω_2) band-limited. The reconstruction problem is to recover $f(s,t)$ from its samples $f(s_{i_1},t_{i_2})$, $i_l=1,2,\cdots,m_l$, $l=1,2$, where the sampling points are selected from $[-T_1,T_1]\times[-T_2,T_2]$ for some T_1, $T_2>0$.

Let

$$S_k=\{(s_{ki_1},t_{ki_2})\in[-T_1,T_1]\times[-T_2,T_2]: i_l=1,2,\cdots,m_{lk},\, l=1,2\},\quad |k|\le K,$$

be a set of arbitrarily fixed $m_{1k}m_{2k}$ distinct points, where

$$\sum_{k=-K}^{K} m_{1k}m_{2k}=m_1m_2. \tag{4.3}$$

Similar to the interpolant $\Psi_m(t)$ in the 1-D case, we have the following $\Psi_{m_1m_2}(s,t)$ for the reconstruction of $f(s,t)$:

$$\Psi_{m_1m_2}(s,t)=\sum_{k=-K}^{K}\sum_{i_1=1}^{m_{1k}}\sum_{i_2=1}^{m_{2k}} a_{ki_1i_2}\frac{\sin B_{1k}(s-s_{ki_1})}{s-s_{ki_1}}\frac{\sin B_{2k}(t-t_{ki_2})}{t-t_{ki_2}}e^{-j(sC_{1k}+tC_{2k})}, \tag{4.4}$$

where $a_{ki_1i_2}$ satisfy the following system

$$\sum_{k=-K}^{K}\sum_{i_1=1}^{m_{1k}}\sum_{i_2=1}^{m_{2k}} a_{ki_1i_2}\frac{\sin B_{1k}(s_{n_1}-s_{ki_1})}{s_{n_1}-s_{ki_1}}\frac{\sin B_{2k}(t_{n_2}-t_{ki_2})}{t_{n_2}-t_{ki_2}}e^{-j(s_{n_1}C_{1k}+t_{n_2}C_{2k})}=f(s_{n_1},t_{n_2}), \tag{4.5}$$

for $n_l=1,2,\cdots,m_l$ and $l=1,2$.

We next estimate the error bound and analyze the critical region of $\Psi_{m_1m_2}(s,t)$. Similar to the assumption (3.4) in the 1-D case, we assume that

$$\frac{m_{lk}}{B_{lk}}=r_l,\quad l=1,2,\ \text{and}\ k=-K,-K+1,\cdots,K, \tag{4.6}$$

where r_1 and r_2 are constants. Thus, by (4.3), we have

$$r_1 r_2 \sum_{k=-K}^{K} B_{1k} B_{2k} = \sum_{k=-K}^{K} m_{1k} m_{2k} = m_1 m_2,$$

and, therefore,

$$r_1 r_2 = \frac{m_1 m_2}{\sum_{k=-K}^{K} B_{1k} B_{2k}}. \tag{4.7}$$

Then, we have the following theorem on the error bound of $\Psi_{m_1 m_2}(t)$.

Theorem 2 *Consider a function $f(s,t)$ of the form (4.2). For all $k = -K, -K+1, \cdots, K$, if*

(i) $f_k(s,t) \in L^1(\mathbf{R})$, or

(ii) $\hat{f}_k(\omega_1, \omega_2)$ is second-order differentiable in $[-B_{1k}, B_{1k}] \times [-B_{2k}, B_{2k}]$,

and the coefficient matrix for unknowns $a_{ki_1i_2}$ in (4.5) is of full rank, then

$$|f(s,t) - \Psi_{m_1 m_2}(s,t)| \le O \sum_{k=-K}^{K} \left(\left(\frac{2e\tau_1}{r_1} \right)^{m_{1k}} + \left(\frac{2e\tau_2}{r_2} \right)^{m_{2k}} \right), \quad \text{for } |s| \le \tau_1, |t| \le \tau_2, \tag{4.8}$$

where $\tau_l \ge T_l$ for $l = 1, 2$, O is a positive constant and r_1, r_2 are as in (4.6).

Since the proof of Theorem 2 is similar to that of Theorem 1, it is omitted. In the uniform multiband case, the estimate in (4.8) can be simplified further.

Corollary 2 *If the same conditions stated in Theorem 2 are satisfied and if $B_{lk} = B_l$, for $|k| \le K$ and $l = 1, 2$, then*

$$|f(s,t) - \Psi_{m_1 m_2}(s,t)| \le O \left(\left(\frac{2e\tau_1}{r_1} \right)^{r_1 B_1} + \left(\frac{2e\tau_2}{r_2} \right)^{r_2 B_2} \right), \quad \text{for } |s| \le \tau_1, |t| \le \tau_2. \tag{4.9}$$

Based on error bounds (4.8) and (4.9), the critical value for $\Psi_{m_1 m_2}$ is

$$\Gamma_{\Psi_{m_1 m_2}} = r_1 r_2 / (4e^2).$$

By using (2.11) and (4.7), we can relate this critical value to that of the MMSE estimator $\Phi_{m_1 m_2}$ in (2.6) as

$$\Gamma_{\Psi_{m_1 m_2}} = \frac{m_1 m_2}{4e^2 \sum_{k=-K}^{K} B_{1k} B_{2k}} = \frac{\Omega_1 \Omega_2}{\sum_{k=-K}^{K} B_{1k} B_{2k}} \Gamma_{\Phi_{m_1 m_2}},$$

so that the gain factor is

$$\gamma_3 \triangleq \frac{\Omega_1 \Omega_2}{\sum_{k=-K}^{K} B_{1k} B_{2k}}.$$

It is clear from (4.1) that $\gamma_3 \ge 1$. Moreover, if the band $[-\Omega_1, \Omega_1] \times [-\Omega_2, \Omega_2]$ is not fully occupied, the gain factor $\gamma_3 > 1$. Thus, we conclude the new algorithm is better than the MMSE estimator for (Ω_1, Ω_2) band-limited signals with a multiband structure.

4.2 Real Multiband Signals

When $f_k(s,t)$ and $f(s,t)$ in (4.2) are real signals, we can find a more efficient reconstruction algorithm. The $f(s,t)$ can be represented as

$$f(s,t) = \sum_{k=0}^{K} f_k(s,t)\cos(sC_{1k} + tC_{2k}).$$

Note that its spectrum $\hat{f}(\omega_1,\omega_2)$ has the symmetry with respect to the origin, i.e

$$\hat{f}(\omega_1,\omega_2) = \hat{f}(-\omega_1,-\omega_2).$$

For $k = 0, 1, \cdots, K$, we use S_k to denote the set of auxiliary sampling points and

$$\sum_{k=0}^{K} m_{1k}m_{2k} = m_1 m_2.$$

Then, we can use the following interpolant as an approximation for the real multiband signal $f(s,t)$:

$$\tilde{\Psi}_{m_1m_2}(s,t) = \sum_{k=0}^{K}\sum_{i_1=1}^{m_{1k}}\sum_{i_2=1}^{m_{2k}} a_{ki_1i_2}\frac{\sin B_{1k}(s-s_{ki_1})}{s-s_{ki_1}}\frac{\sin B_{2k}(t-t_{ki_2})}{t-t_{ki_2}}\cos(sC_{1k}+tC_{2k}),$$

where coefficients $a_{ki_1i_2}$ satisfy the following system

$$\sum_{k=0}^{K}\sum_{i_1=1}^{m_{1k}}\sum_{i_2=1}^{m_{2k}} a_{ki_1i_2}\frac{\sin B_{1k}(s_{n_1}-s_{ki_1})}{s_{n_1}-s_{ki_1}}\frac{\sin B_{2k}(t_{n_2}-t_{ki_2})}{t_{n_2}-t_{ki_2}}\cos(s_{n_1}C_{1k}+t_{n_2}C_{2k}) = f(s_{n_1},t_{n_2}),$$

for $n_l = 1, 2, \cdots, m_l$ and $l = 1, 2$. The error bound on the interpolant $\tilde{\Psi}_{m_1m_2}(s,t)$ is

$$|f(s,t) - \tilde{\Psi}_{m_1m_2}(s,t)| \le O\sum_{k=0}^{K}\left(\left(\frac{2e\tau_1}{\tilde{r}_1}\right)^{m_{1k}} + \left(\frac{2e\tau_2}{\tilde{r}_2}\right)^{m_{2k}}\right), \text{ for } |s|\le\tau_1, |t|\le\tau_2,$$

where $\tau_l \ge T_l$ for $l = 1, 2$, O the same as in (4.8) and

$$\tilde{r}_1\tilde{r}_2 = \frac{m_1m_2}{\sum_{k=0}^{K} B_{1k}B_{2k}}. \tag{4.10}$$

By using (2.11), (4.7) and (4.10), we can compute the critical value for this case as

$$\Gamma_{\tilde{\Psi}_{m_1m_2}} = \frac{\tilde{r}_1\tilde{r}_2}{4e^2} = \frac{\tilde{r}_1\tilde{r}_2}{r_1r_2}\frac{r_1r_2}{4e^2} = \frac{\sum_{k=-K}^{K} B_{1k}B_{2k}}{\sum_{k=0}^{K} B_{1k}B_{2k}}\Gamma_{\Psi_{m_1m_2}} = \frac{\Omega_1\Omega_2}{\sum_{k=0}^{K} B_{1k}B_{2k}}\Gamma_{\Phi_{m_1m_2}}.$$

Therefore, we have the gain factor

$$\gamma_4 = \frac{\Omega_1\Omega_2}{\sum_{k=0}^{K} B_{1k}B_{2k}}.$$

If the bandwidth B_0 of the baseband is small, we have

$$\frac{\sum_{k=-K}^{K} B_{1k}B_{2k}}{\sum_{k=0}^{K} B_{1k}B_{2k}} \approx 2.$$

Consequently, $\Gamma_{\tilde{\Psi}_{m_1 m_2}} \approx 2\Gamma_{\Psi_{m_1 m_2}} \geq 2\Gamma_{\Phi_{m_1 m_2}}$ and $\gamma_4 \geq 2$. Note also that if the signal has symmetric spectrum with respect to both ω_1 and ω_2 axes, it can be expressed as

$$f(s,t) = \sum_{k=0}^{K} f_k(s,t)\cos(sC_{1k})\cos(tC_{2k}).$$

It is possible to modify the above algorithm so that it achieves a gain factor $\gamma_5 \geq 4$.

5 Numerical Experiments

We use numerical examples to demonstrate the performance the proposed algorithms.

Test Problem 1: 1-D multiband signal.

The test signal is chosen to be the modulated real signals

$$f(t) = f_0(t) + 0.5f_1(t)\cos(C_1 t),$$

with the Fourier spectrum

$$\hat{f}_k(\omega) = \begin{cases} \pi \sin(\alpha_k|\omega|), & |\omega| \leq B_k \\ 0 & |\omega| > B_k, \end{cases}$$

where $k = -1, 0, 1$, and α_k and B_k are positive constants. Since $f(t)$ is real, $\hat{f}_k(-\omega) = \hat{f}_k(\omega)$. In the experiment, we choose

$$\alpha_0 = 4\pi, \quad \alpha_1 = 6\pi,$$

and

$$\Omega = 4\pi, \quad B_0 = \frac{\pi}{8}, \quad C_1 = \Omega - B_1,$$

where B_1 be a parameter ranging from 0 to $31\pi/16$. Note that, when $B_1 = 31\pi/16$, $B_0 + 2B_1 = \Omega$ so that the band $[-\Omega, \Omega]$ is fully occupied. We observe the function $f(t)$ at uniformly sampled points $t = n/10$ with $n = -10, -9, \cdots, 9$ so that the total number of sampling points is 20. The auxiliary sampling point sets are chosen as subsets of S with $S_1 \cup S_2 = S$.

We compute $\tilde{\Psi}_m$ for the reconstruction of $f(t)$. The critical value for this case is

$$\Gamma_{\tilde{\Psi}_{20}} = \frac{20}{2e(B_0 + B_1)} = \frac{10}{e(\pi/8 + B_1)},$$

which is a function of B_1. The curve of $\Gamma_{\tilde{\Psi}_{20}}$ via B_1 is shown in Fig. 5. The critical point for the MMSE estimator is

$$\Gamma_{\Phi_{20}} = \frac{20}{2e(4\pi)} = \frac{5}{2e\pi},$$

which corrresponds to the constant line as shown in Fig. 5. We can clearly see the improvement of our proposed algorithm when the bandwidth B_1 becomes smaller and the band $[-\Omega, \Omega]$ is less fully utilized.

To give a more clear performance comparison of various methods, we applied the MMSE estimator $\Phi_{20}(t)$ and the interpolant $\tilde{\Psi}_{20}(t)$ to two test signals with $B_1 = \pi/8$ and $B_1 = 31\pi/16$ and plotted the results in Figs. 6-9. In all these figures, we show the true signal $f(t)$ in (a), its Fourier spectrum $\hat{f}(\omega)$ in (b), the reconstructed function ($\tilde{\Psi}_{20}(t)$ or $\Phi_{20}(t)$) in (c) and the corresponding error ($|\tilde{\Psi}_{20}(t) - f(t)|$ or $|\Phi_{20}(t) - f(t)|$) in (d). In subplot (d), we also indicate the critical region by labeling its two boundary points as "critical point". When $B_1 = \pi/8$, the signal $f(t)$ consists of three narrow bands. When $B_1 = 31\pi/16$, the signal $f(t)$ is in fact a full-band signal. By comparing the results in Figs. 6 and 7 and those in Figs. 8 and 9, we can clearly see that the proposed method with $\tilde{\Psi}_{20}(t)$ performs much better than the MMSE estimator $\tilde{\Phi}_{20}(t)$ in both cases. Besides, the proposed algorithm performs better when the bandwidth is not fully occupied.

Test Problem 2: 2-D multiband signal.

The 2-D test signal is a $(4\pi, 4\pi)$ band-limited real signal of the form

$$f(s,t) = f_0(s,t) + 0.25 f_1(s,t)\cos(C_{11}s + C_{12}t),$$

where $f_k(s,t)$ are (B_{1k}, B_{2k}) band-limited with $B_{1k} = B_{2k} = \pi/4$ for $k = 0, 1$, $C_{11} = C_{12} = 4\pi - \pi/4 = 15\pi/4$. The contour plot of the Fourier spectrum $\hat{f}(\omega_1, \omega_2)$ is given in Fig. 10(a) and the original signal $f(s,t)$ is shown in Fig. 10(b). We choose $m_1 = m_2 = 20$, $m_{10} = m_{11} = 10$ and $m_{20} = m_{21} = 20$. The sampling point set is $S = \{(n_1/10, n_2/10) : \text{for } n_i = -10, -9, \cdots, 9 \text{ for } i = 1, 2\ \}$, which is concentrated in $[-1,1] \times [-1,1]$. The auxiliary sampling point sets S_0 and S_1 are also chosen as subsets of S. The reconstruction $\Phi_{20,20}(s,t)$ from the MMSE estimator and the reconstruction $\tilde{\Psi}_{20,20}(s,t)$ from our proposed method are shown in Figs. 11 (a) and (b), respectively. We can clearly see that the new method gives a more accurate result over a larger domain. We also show the absolute error of these two methods in Figs. 12 and 13 with both surface and contour plots. The improvement is clear from these plots.

6 Conclusions

We proposed a new reconstruction algorithm for a band-limited signal with a multiband structure from its finite samples. The concept of critical regions and values for a reconstruction algorithm was introduced for the performance measure. Based on this criterion, we can clearly see the improvement of our new algorithm for band-limited/multiband signals over the MMSE estimator for general band-limited signals. We also gave numerical experiments to support the theoretical derivation.

Appendix: Proof of Theorem 1

Let $\mathbf{a}$ denote the solution vector for the system (3.3), and A be the coefficient matrix. Let $\mathbf{f}$ be the constant vector with components $f(t_n)$ in (3.3). Then, we can write (3.3) as

$$A\mathbf{a} = \mathbf{f}. \tag{A.1}$$

Let $\mathbf{a}^{(\alpha)}$ be the Tikhonov regularization solution of the system (A.1) with parameter α, i.e.,

$$\mathbf{a}^{(\alpha)} = \frac{A^*\mathbf{f}}{A^*A + \alpha I}, \tag{A.2}$$

where A^* is the complex conjugate of the matrix A and I is the $m \times m$ identity matrix. Then, see [27], [29],

$$\|\mathbf{a} - \mathbf{a}^{(\alpha)}\| \leq O_1\sqrt{\alpha}, \tag{A.3}$$

where O_1 is a constant which only depends on the signal f. For each k with $-K \leq k \leq K$, let b_{ki} satisfy the following system

$$\sum_{i=1}^{m_k} b_{ki}\frac{\sin B_k(t_{kl} - t_{ki})}{t_{kl} - t_{ki}} = f_k(t_{kl}), \text{ for } l = 1, 2, \cdots, m_k. \tag{A.4}$$

Let $\mathbf{b}$ denote the vector with components b_{ki} for all possible k, i. From $\mathbf{b}$ we have the MMSE estimator

$$\Phi_{m_k}(t) = \sum_{i=1}^{m_k} b_{ki}\frac{\sin B_k(t - t_{ki})}{t - t_{ki}}.$$

Then, by applying the error estimate (2.4) to the kth B_k band-limited signal $f_k(t)$ of $f(t)$,

$$|f_k(t) - \Phi_{m_k}(t)| < O\sqrt{E(f_k)}r\left(\frac{2e\tau}{r}\right)^{m_k}, \text{ for } t \in [-\tau, \tau], \tag{A.5}$$

where $\tau \geq T$ and r is defined in (3.4). Since $t_n \in [-T, T]$, we have

$$|f_k(t_n) - \Phi_{m_k}(t_n)| < O\sqrt{E(f_k)}r\left(\frac{2eT}{r}\right)^{m_k}, \text{ for } n = 1, 2, \ldots m.$$

Therefore,

$$\begin{aligned} |(A\mathbf{b})(n) - f(t_n)| &= |\sum_{k=-K}^{K} \Phi_{m_k}(t_n)e^{-jt_nC_k} - f(t_n)| \\ &\leq \sum_{k=-K}^{K} |\Phi_{m_k}(t_n) - f_k(t_n)| \\ &\leq Or\sum_{k=-K}^{K}\left(\frac{2eT}{r}\right)^{m_k}, \text{ for } n = 1, 2, \ldots m, \end{aligned} \tag{A.6}$$

where O is as before. Let

$$\mathbf{b}^{(\alpha)} \triangleq \frac{A^*A\mathbf{b}}{A^*A + \alpha I}.$$

Then,

$$\|\mathbf{b} - \mathbf{b}^{(\alpha)}\| \leq O_2\sqrt{\alpha}, \tag{A.7}$$

where O_2 is a positive constant which only depends on the signal f. By (A.1), (A.6) and (A.7),

$$\begin{aligned}\|\mathbf{a}^{(\alpha)} - \mathbf{b}^{(\alpha)}\| &= \|\frac{A^*\mathbf{f}}{A^*A + \alpha I} - \frac{A^*A\mathbf{b}}{A^*A + \alpha I}\| \\ &\leq \frac{1}{\alpha}\|A^*(A\mathbf{b} - \mathbf{f})\| \leq \frac{2m}{\alpha} r \sum_{k=-K}^{K} \left(\frac{2eT}{r}\right)^{m_k}.\end{aligned}$$

Therefore,

$$\begin{aligned}\|\mathbf{a} - \mathbf{b}\| &\leq \|\mathbf{a} - \mathbf{a}^{(\alpha)}\| + \|\mathbf{a}^{(\alpha)} - \mathbf{b}^{(\alpha)}\| + \|\mathbf{b} - \mathbf{b}^{(\alpha)}\| \\ &\leq (O_1 + O_2)\sqrt{\alpha} + \frac{2mr}{\alpha} \sum_{k=-K}^{K} \left(\frac{2eT}{r}\right)^{m_k}.\end{aligned}$$

Setting

$$\alpha = m\left(r \sum_{k=-K}^{K} \left(\frac{2eT}{r}\right)^{m_k}\right)^{2/3},$$

we have

$$\|\mathbf{a} - \mathbf{b}\| \leq O\sqrt{m}\left(r \sum_{k=-K}^{K} \left(\frac{2eT}{r}\right)^{m_k}\right)^{1/3}. \tag{A.8}$$

We are now ready to estimate the error of the new algorithm Ψ_m.

$$\begin{aligned}|\Psi_m(t) - f(t)| &\leq |\Psi_m(t) - \sum_{k=-K}^{K} \Phi_{m_k}(t)e^{-jtC_k}| + |\sum_{k=-K}^{K} \Phi_{m_k}(t)e^{-jtC_k} - f(t)| \\ &\leq |\sum_{k=-K}^{K} \sum_{i=1}^{m_k} (a_{ki} - b_{ki}) \frac{\sin B_k(t - t_{ki})}{t - t_{ki}} e^{-jtC_k}| + \sum_{k=-K}^{K} |\Phi_{m_k}(t) - f_k(t)|.\end{aligned}$$

By (A.5) and (A.8), for $t \in [-\tau, \tau]$ with $\tau \geq T$,

$$|\Psi_m(t) - f(t)| \leq O_1 mr \left(\sum_{k=-K}^{K} \left(\frac{2eT}{r}\right)^{m_k}\right)^{1/3} + O_2 r \sum_{k=-K}^{K} \left(\frac{2e\tau}{r}\right)^{m_k}.$$

When τ is significantly larger than T,

$$|\Psi_m(t) - f(t)| \leq Or \sum_{k=-K}^{K} \left(\frac{2e\tau}{r}\right)^{m_k},$$

where O is a constant which only depends on the signal f.

References

[1] M. G. Beaty and M. M. Dodson, "The distribution of sampling rates for signals with equally wide, equally spaced spectral bands," *SIAM J. Appl. Math.*, vol. 53, pp. 893-906, June 1993.

[2] F. J. Beutler, "Error-free recovery of signals from irregularly spaced samples," *SIAM Rev.*, vol. 8, pp. 328-335, Jul. 1966.

[3] J. A. Cadzow, "An extrapolation procedure for band-limited signals," *IEEE Trans. on Acoustics, Speech and Signal Processing*, vol.27, pp.4-12, Feb. 1979.

[4] G. Calvagno and D. C. Munson Jr., "New results on Yen's approach to interpolation from nonuniformly spaced samples", *Proceedings of ICASSP*, pp. 1535-1538, April 1990.

[5] D. S. Chen and J. P. Allebach, "Analysis of error in reconstruction of two-dimensional signals from irregularly spaced samples," *IEEE Trans. on Acoustics, Speech and Signal Processing*, vol. 35, pp. 173-180, Feb. 1987.

[6] R. M. Fitzgerald and C. L. Byrne, "Extrapolation of band-limited signals: A tutorial," in *Signal Processing Theory and Application* (M.Kunt and F.Coulon, eds.), pp. 175-179, Amsterdam: North-Holland, 1980.

[7] R. W. Gerchberg,"Super-resolution through error energy reduction," *Opt. Acta*, vol. 21, No.9, pp.709-720, 1974.

[8] M. Golomb and H. F. Weinberger, "Optimal approximation and error bounds," in *On Numerical Approximation*(R.Langer, ed), pp. 117-190, Madison, WI: University of Wisconsin Press, 1959.

[9] N. E. Hurt, *Phase Retrieval and Zero Crossings*, Kluwer Academic Publisher, Boston, 1989.

[10] A. J. Jerri, "The Shannon sampling theorem–its various extensions and applications: a tutorial review," *Proceedings of The IEEE* Vol. 65, No. 11, Nov. 1977.

[11] D. P. Kolba and T. W. Parks, "Optimal estimation for band-limited signals including time domain considerations," *IEEE Trans. on Acoustics, Speech and Signal Processing*, vol. 31, pp. 113-122, Feb. 1983.

[12] M. A. Kowalski,"Optimal complexity recovery of band and energy-limited signals," *J. Complexity 2*, pp.239-254, 1986.

[13] H. J. Landau, "Extrapolating a band-limited function from its samples taken in a finite interval," *IEEE Trans. on Information Theory*, vol. IT-32, No. 4, July 1986.

[14] L. Levi, "Fitting a bandlimited signal to given points," *IEEE Trans. on Inform. Theory*, vol. 11, pp. 372-376, Jul. 1966.

[15] C. A. Micchelli and T. J. Rivlin,"A survey of optimal recovery," in *Optimal Estimation in Approximation Theory*, (C.A.Micchelli and T.J.Rivlin, Eds), Plenum, New York, 1977.

[16] V. A. Morozov, "The error principle in the solution of operational equations by the regularization method," *USSR Compt. Math. Phys.*, vol. 8, no. 2, 1968.

[17] A. Papoulis,"A new algorithm in spectral analysis and band-limited extrapolation," *IEEE Trans. on Circuits Syst.*, vol.CAS-22, pp.735-742, Sept. 1975.

[18] L. C. Potter and K. S. Arun, "Energy concentration in band-limited extrapolation," *IEEE Trans. on Acoustics, Speech and Signal Processing*, vol. 37, pp. 1027-1041, Jul. 1989.

[19] J. L. C. Sanz and T. S. Huang, "Some aspects of band-limited signal extrapolation: models, discrete approximations and noises," *IEEE Trans. on Acoustics, Speech and Signal Processing*, vol. 31, No.6, Dec. 1983.

[20] H. J. Schlebusch and W. Splettstösser, "On a conjecture of J.L.C.Sanz and T.S.Huang," *IEEE Trans. on Acoustics, Speech and Signal Processing*, vol. 33, Oct. 1985.

[21] D. Slepian, "Prolate spheroidal wave functions, Fourier analysis, and uncertainty-V: The discrete case," *Bell Syst. Tech. J.*, vol. 57, pp. 1371-1430, May-June 1978.

[22] D. Slepian, H. O. Pollak, and H. J. Landau, "Prolate spheroidal wave functions I, II," *Bell Syst. Tech. J.*, vol. 40, pp.43-84, Jan. 1961.

[23] A. N. Tikhonov and V. Y. Arsenin, *Solutions of Ill-Posed Problems*, Washington, D.C.: Winston, 1977.

[24] R. G. Vaughan, N. L. Scott and D. R. White, "The theory of bandpass sampling," *IEEE Trans. on Signal Processing*, vol. 39, pp. 1973-1984, Sept. 1991.

[25] X.-G. Xia, Z. Zhang and C. M. Lo, "Error analysis of the MMSE estimator for multidimensional band-limited extrapolations from finite samples," to appear in *Signal Processing*, 1994.

[26] W. Y. Xu and C. Chamzas,"On the extrapolation of band-limited functions with energy constraints," *IEEE Trans. on Acoustics, Speech and Signal Processing*, vol. 31, No.5, Oct. 1983.

[27] J. L. Yen, "On nonuniform sampling of bandlimited signals," *IRE Trans. Circuit Theory*, vol. 3, pp. 251-257, Dec. 1956.

[28] D. C. Youla, "Generalized image restoration by the method of alternating orthogonal projections," *IEEE Trans. on Circuits Syst.*, vol.CAS-25, pp.694-701, Sept. 1978.

[29] X. W. Zhou and X.-G. Xia, "The extrapolations of high dimensional band-limited signals," *IEEE Trans. on Acoustics, Speech and Signal Processing*, vol. 37, Oct. 1989.

Figure Captions

Figure 1: Fourier spectrum of a multiband signal.

Figure 2: Critical points in (a) 1-D and (b) 2-D cases.

Figure 3: Fourier spectrum of a modulated real signal.

Figure 4: Occupied bands in the frequency domain of 2-D multiband signals.

Figure 5: The critical value curves via B_1 for the algorithm $\tilde{\Psi}_{20}$ and the MMSE estimator Φ_{20}.

Figure 6: Results with $\Phi_{20}(t)$ for $B_1 = \pi/8$.

Figure 7: Results with $\tilde{\Psi}_{20}(t)$ for $B_1 = \pi/8$.

Figure 8: Results with $\Phi_{20}(t)$ for $B_1 = 31\pi/16$.

Figure 9: Results with $\tilde{\Psi}_{20}(t)$ for $B_1 = 31\pi/16$.

Figure 10: (a) The contour plot of $\hat{f}(\omega_1, \omega_2)$ and (b) the surface plot of the exact $f(s,t)$.

Figure 11: The reconstructions: (a) $\Phi_{20,20}(s,t)$ and (b) $\tilde{\Psi}_{20,20}(s,t)$.

Figure 12: The error $err_2 = |\Phi_{20,20}(s,t) - f(s,t)|$: (a) the surface plot and (b) the contour plot.

Figure 13: The error $err_1 = |\tilde{\Psi}_{20,20}(s,t) - f(s,t)|$: (a) the surface plot and (b) the contour plot.

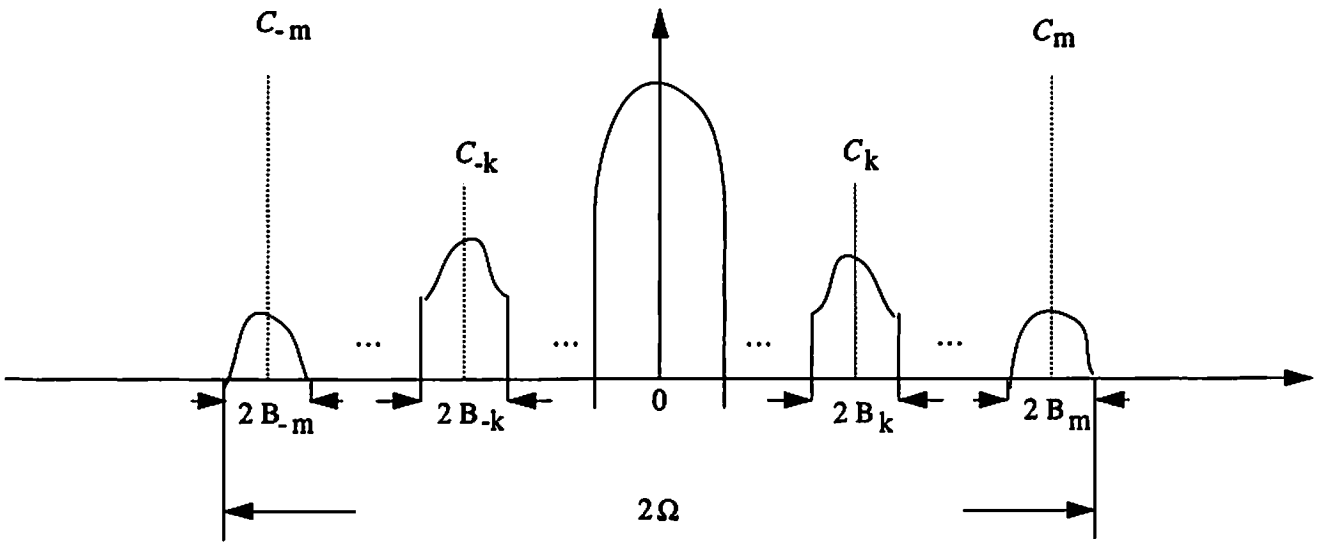

Figure 1: Fourier spectrum of a multiband signal.

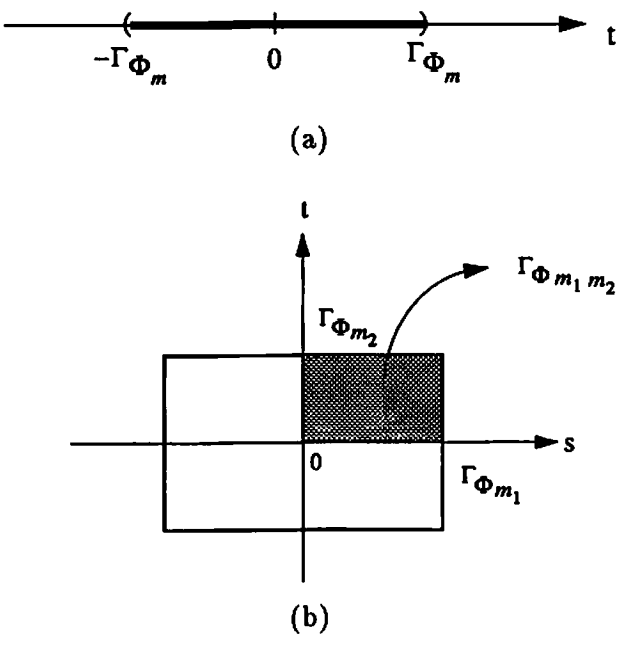

Figure 2: Critical points in (a) 1-D and (b) 2-D cases.

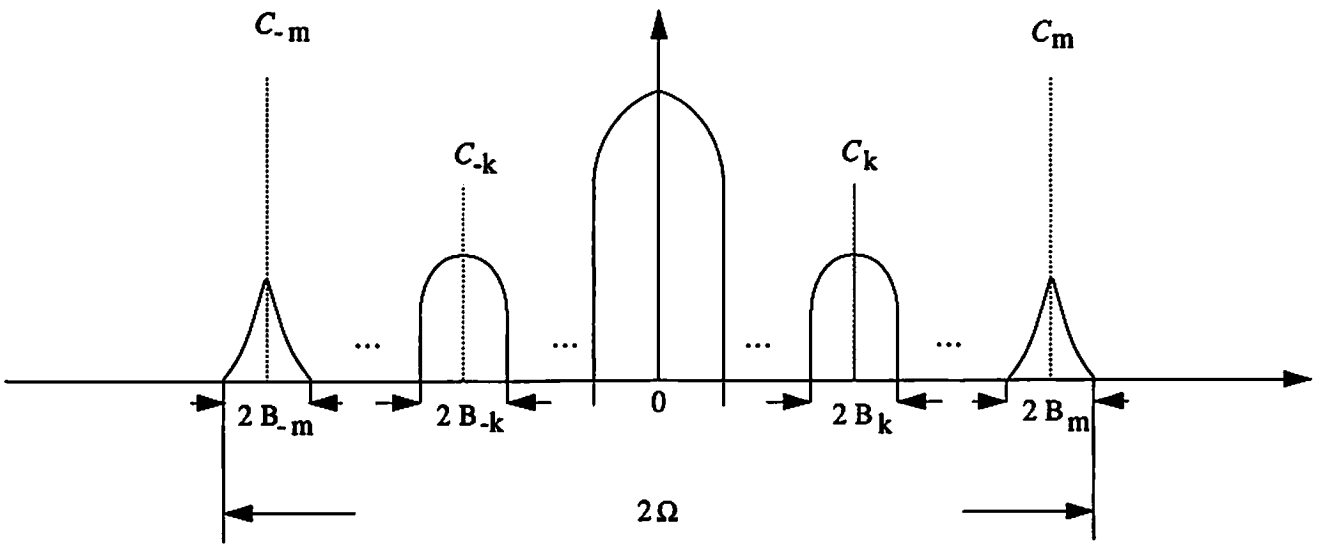

Figure 3: Fourier spectrum of a modulated real signal.

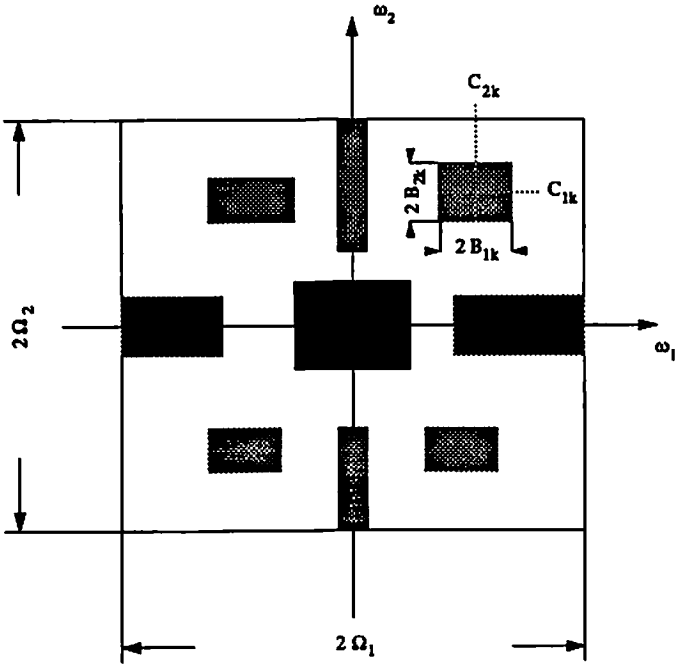

Figure 4: Occupied bands in the frequency domain of 2-D multiband signals.

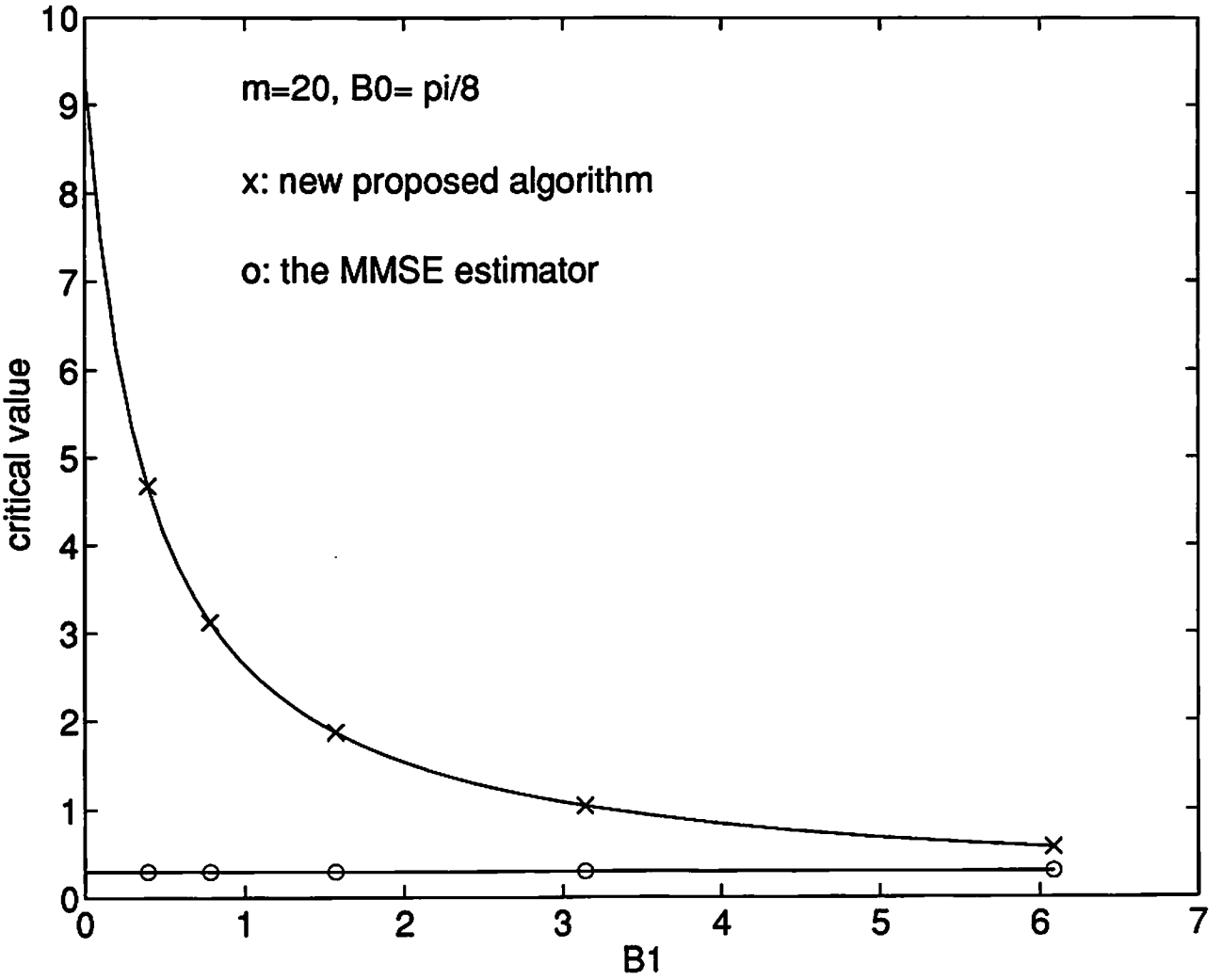

Figure 5: The critical value curves via B_1 for the $\tilde{\Psi}_{20}$ and the MMSE estimator Φ_{20}.

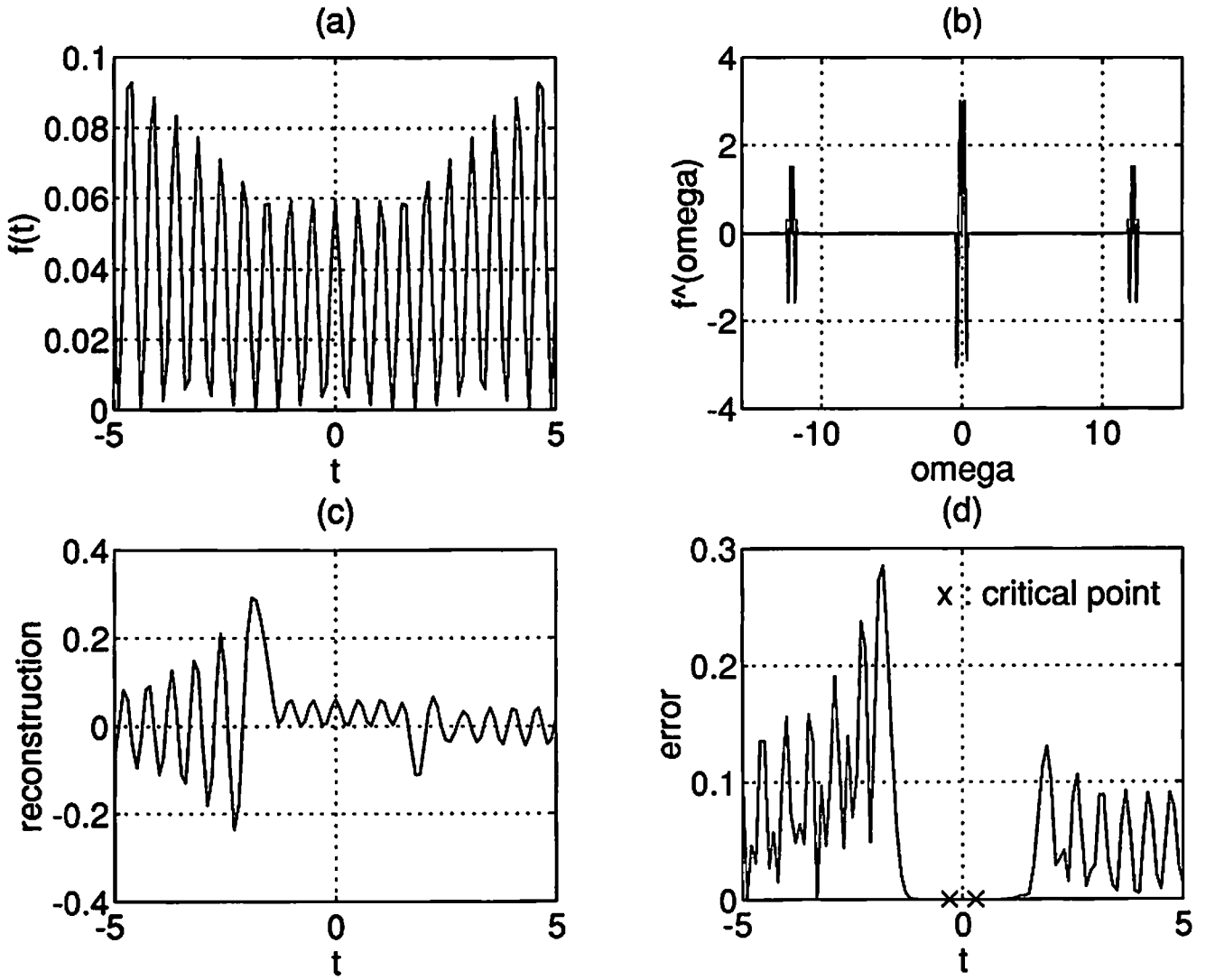

Figure 6: Results with $\Phi_{20}(t)$ for $B_1 = \pi/8$.

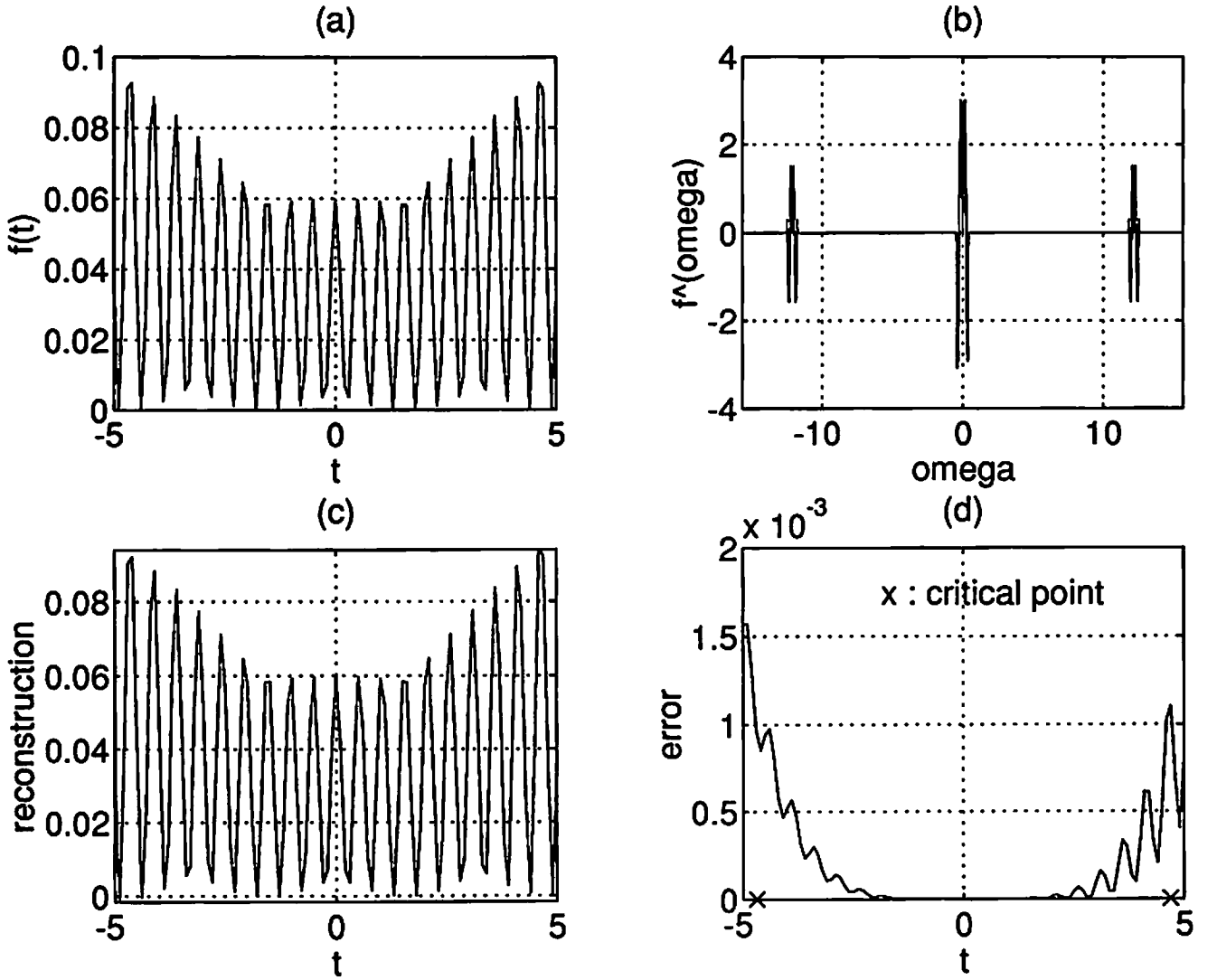

Figure 7: Results with $\tilde{\Psi}_{20}(t)$ for $B_1 = \pi/8$.

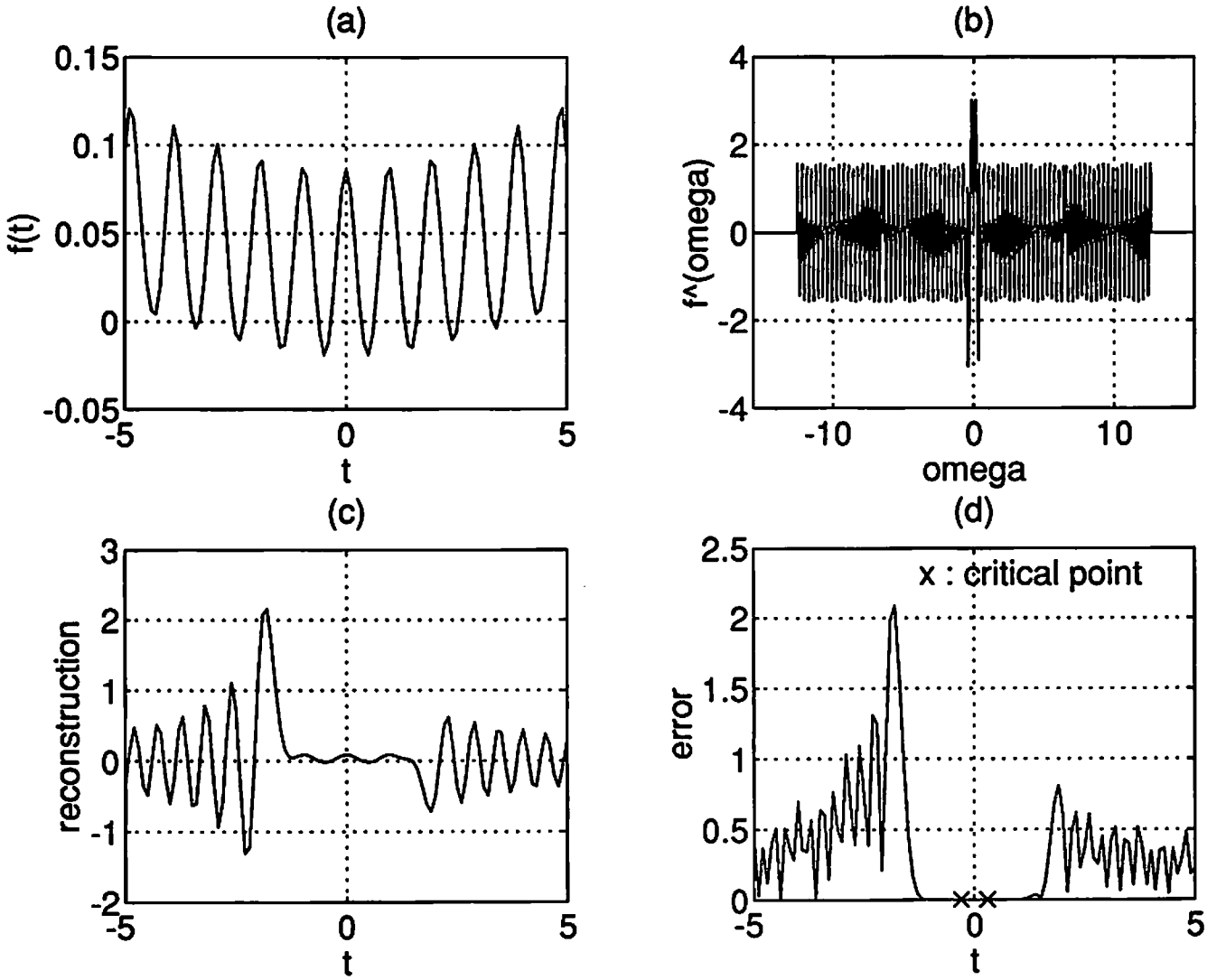

Figure 8: Results with $\Phi_{20}(t)$ for $B_1 = 31\pi/16$.

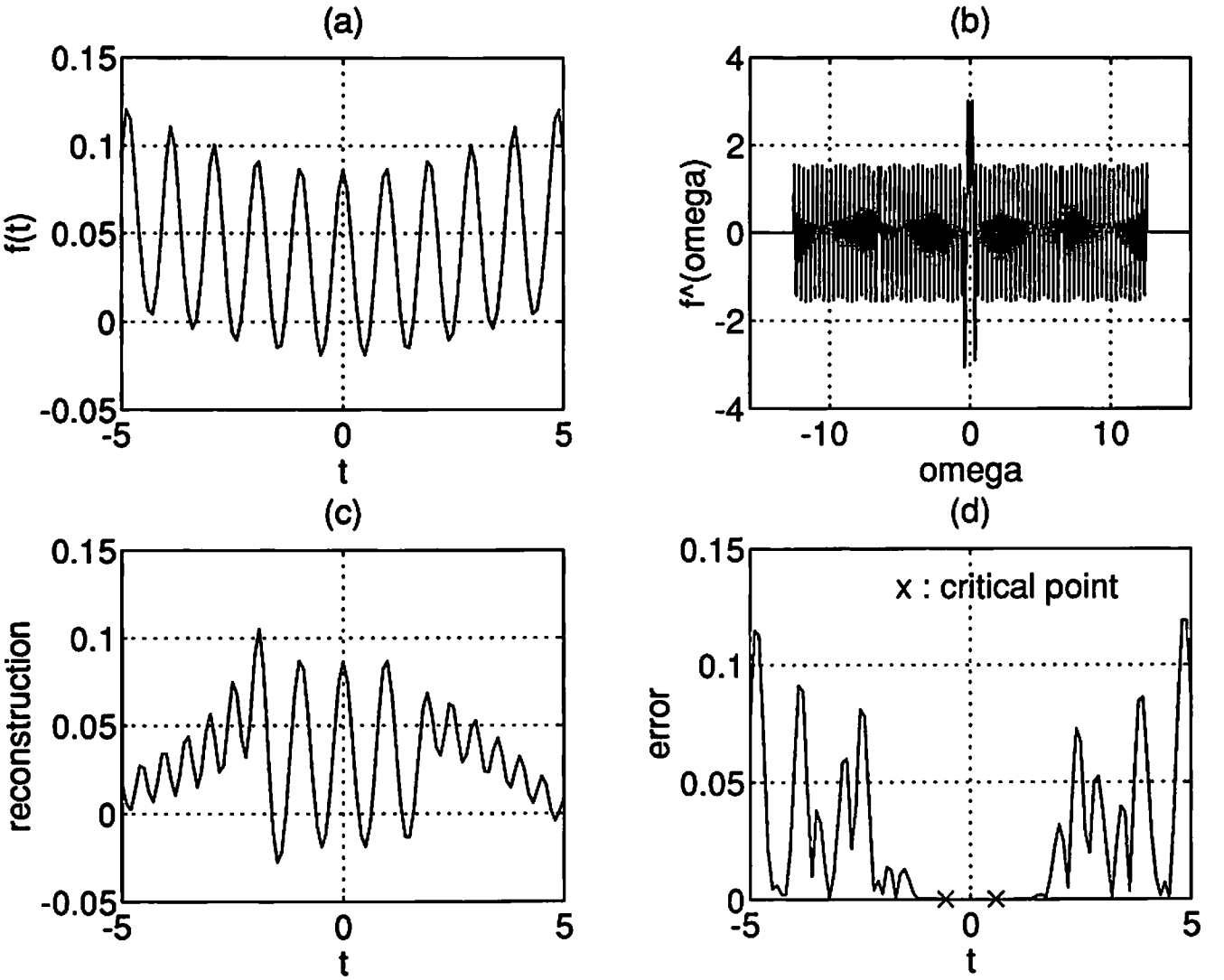

Figure 9: Results with $\tilde{\Psi}_{20}(t)$ for $B_1 = 31\pi/16$.

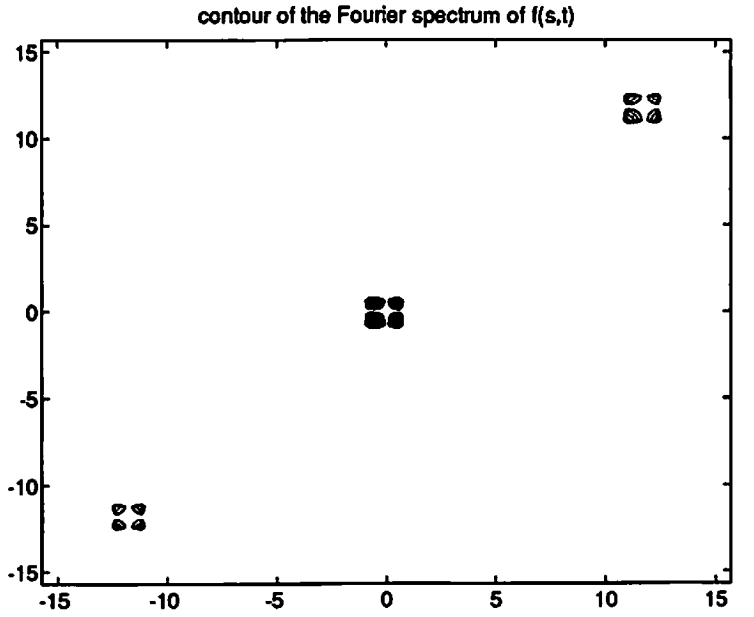

(a)

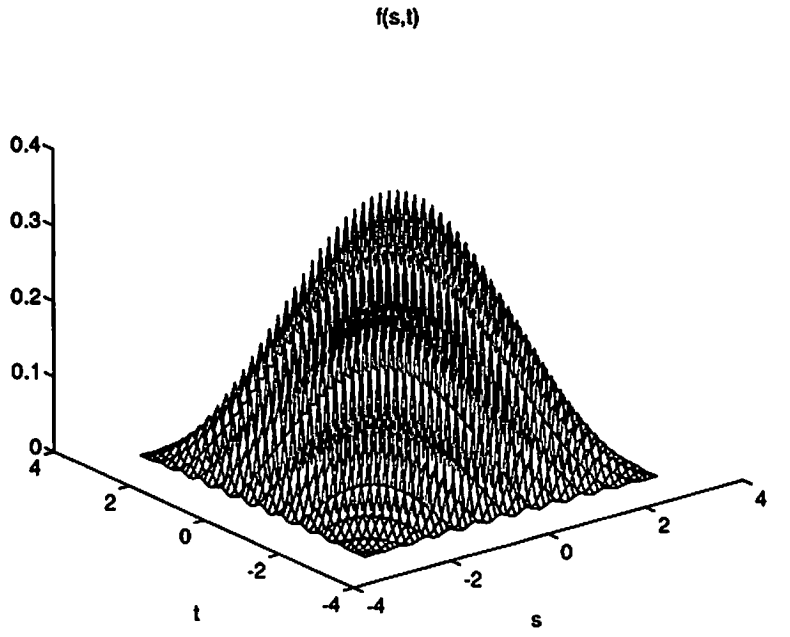

(b)

Figure 10: (a) The contour plot of $\hat{f}(\omega_1, \omega_2)$ and (b) the surface plot of the exact $f(s,t)$.

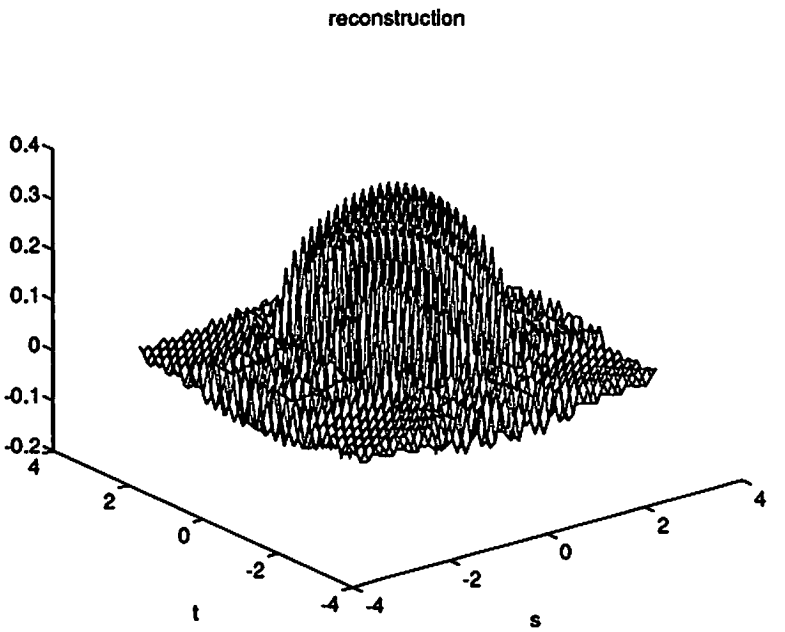

(a)

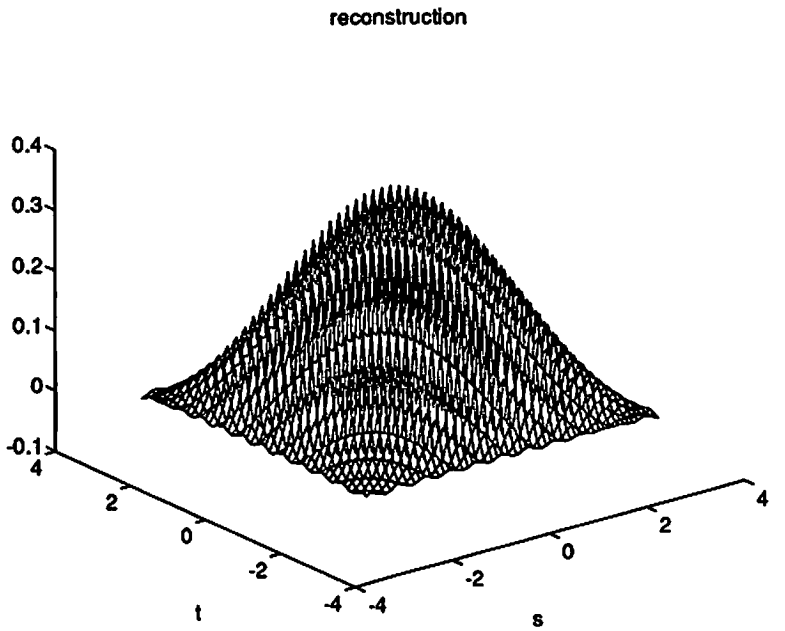

(b)

Figure 11: The reconstructions: (a) $\Phi_{20,20}(s,t)$ and (b) $\tilde{\Psi}_{20,20}(s,t)$.

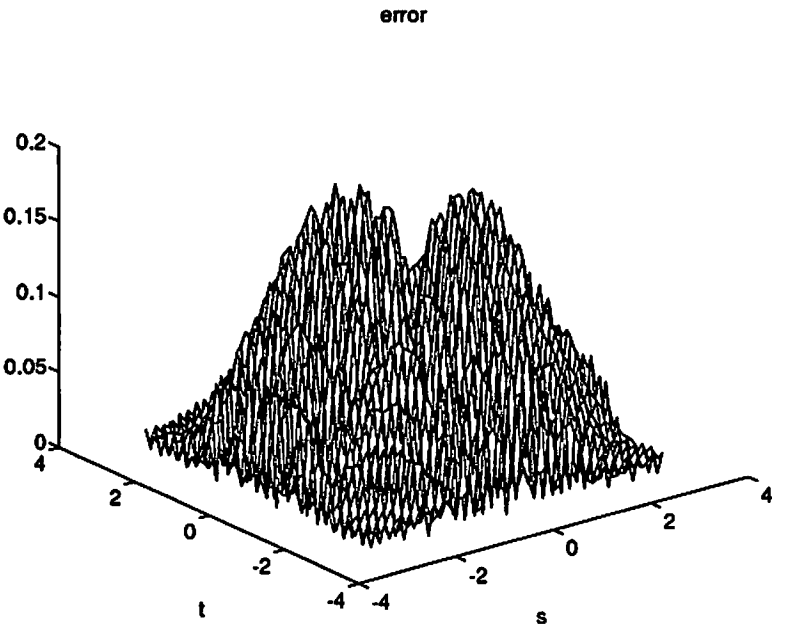

(*a*)

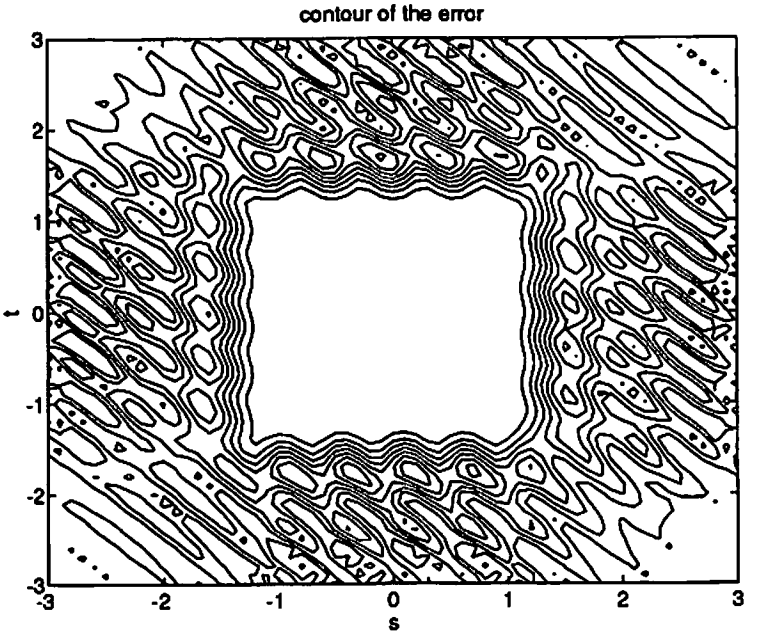

(*b*)

Figure 12: The error $err_2 = |\Phi_{20,20}(s,t) - f(s,t)|$: (a) the surface plot and (b) the contour plot.

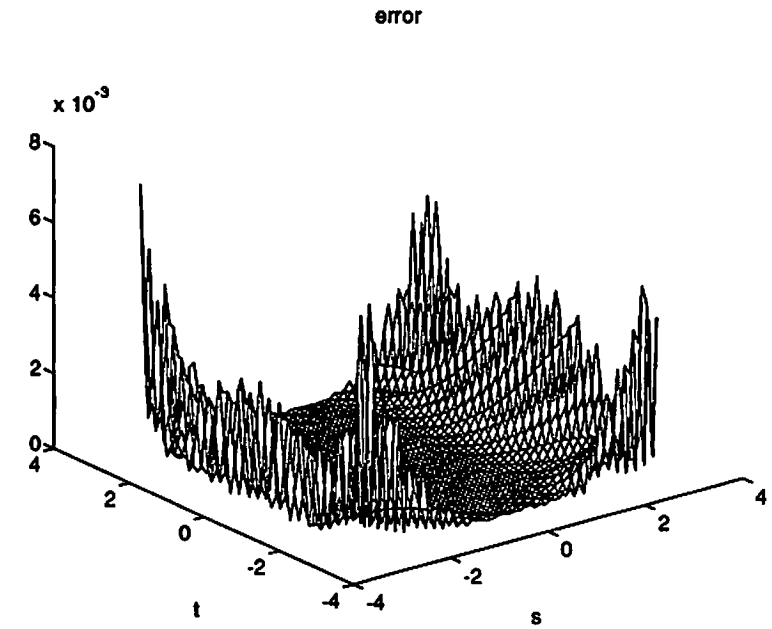

(*a*)

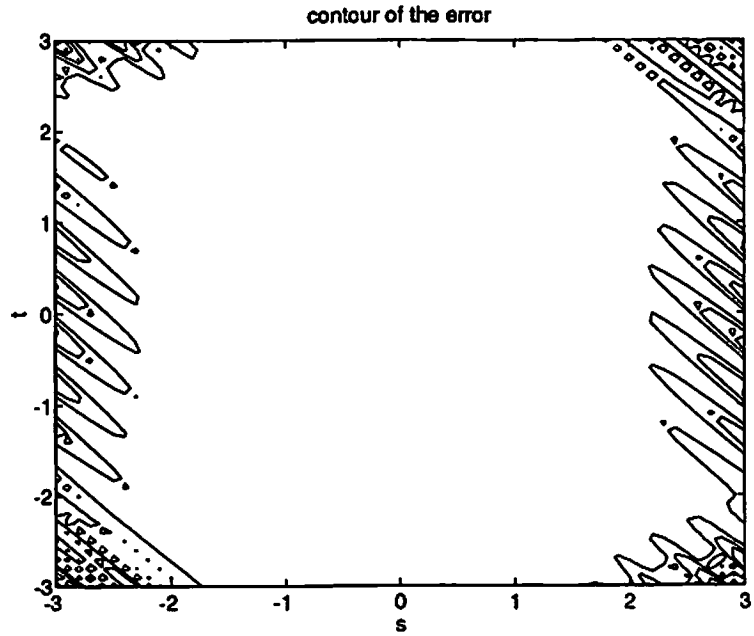

(*b*)

Figure 13: The error $err_1 = |\tilde{\Psi}_{20,20}(s,t) - f(s,t)|$: (a) the surface plot and (b) the contour plot.